11-year solar cycle influence on OH (3-1) nightglow observed by OSIRIS

Journal of Atmospheric and Solar–Terrestrial Physics 229 (2022) 105831

Contents lists available at ScienceDirect

Journal of Atmospheric and Solar–Terrestrial Physics

journal homepage: www.elsevier.com/locate/jastp

Research paper

11-year solar cycle influence on OH (3-1) nightglow observed by OSIRIS

Anqi Li [a,*], Donal P. Murtagh [a], Adam E. Bourassa [b], Douglas A. Degenstein [b], Chris Z. Roth [b]

[a] Chalmers university of technology, Department of Space, Earth and Environment, Gothenburg, Sweden
[b] Institute of Space and Atmospheric Studies, University of Saskatchewan, Saskatoon, Canada

ARTICLE INFO

Keywords:
Airglow
11-year solar cycle
Hydroxyl layer

ABSTRACT

In the mesosphere, the vibrationally excited hydroxyl layer is sensitive to changes in incoming solar flux. An enhanced photodissociation of molecular oxygen will lead to more atomic oxygen production, thus we expect the OH layer emission rate to be positively with the Lyman-α flux and the emission height to be negatively correlated. The Optical Spectrograph and InfraRed Imager System (OSIRIS) has recorded the Meinel band centred at 1.53 μm from 2001 to 2015. In this study, we show how the 11-year solar cycle signature manifests itself in this data set, in terms of OH zenith emission rate and emission height. As expected, the emission height is negatively correlated with the Lyman-α flux at all latitudes. The zenith emission rate is positively correlated with the Lyman-α flux at most latitudes except near the equator. By the means of a time dependent photochemical model, we show that the changing local time sampling of the Odin satellite was the cause of the observed distortion of the solar cycle signature near the equator.

1. Introduction

The mesosphere and lower thermosphere (MLT) is particularly sensitive to changes in solar flux since photolysis processes play an important role in the chemistry of this atmospheric region. The vibrationally excited hydroxyl OH, concentrated near the mesopause, is one of the species strongly influenced by photochemistry. While its removal relies on quenching processes, its production primary relies on the recombination of hydrogen atom and ozone.

$$H + O_3 \rightarrow OH* + O_2. \quad \text{(R1)}$$

Since mesospheric O_3 exhibits a prominent diurnal cycle, OH_*[1] follows accordingly — its concentration increasing sharply around the sunset (Allen et al., 1984).

Furthermore, if one considers that ozone is in photochemical equilibrium, the production rate of OH_*, given by

$$P = k_{H+O_3}[H][O_3], \quad (1)$$

$$\text{with } [O_3] = \frac{k_{O+O_2+M}[O][O_2][M]}{k_{H+O_3}[H]}, \quad (2)$$

is controlled by temperature and the concentration of atomic oxygen (e.g. Marsh et al., 2006; Grygalashvyly, 2015), which is mainly produced by the photodissociation of molecular oxygen. Thus, the long-term behaviour of OH_* depends on changes in incoming solar flux. Grygalashvyly et al. (2014) and Sonnemann et al. (2015) have performed modelling studies to investigate the long-term trend in the OH_* layer. They showed that the 11-year solar cycle in Lyman-α flux variation was imprinted in the model results for both the layer height and the number density. Several independent studies based on ground-based monitoring of the OH_* airglow also showed that an 11-year cycle signature was present in their data sets (e.g. Fukuyama, 1977; Pertsev and Perminov M. Obukhov, 2008; Clemesha et al., 2005).

Satellite observations offer a much better geographical coverage and yield information on the layer height. Liu and Shepherd (2006a), von Savigny (2015), Teiser and von Savigny (2017), García-Comas et al. (2017) and Gao et al. (2016) have used various techniques to study the correlation between the OH_* emission rate and/or emission height and the solar flux. However, using space-borne observations to investigate long-term changes is not easy since the lifespan of most missions is not long enough. Liu and Shepherd (2006a) found a negative correlation between the emission height of the OH (8-3) band and the F10.7 cm flux based on WINDII[2] data from November 1991 to August 1997. However, von Savigny (2015) found little evidence for this negative correlation based on the SCIAMACHY[3] OH(3-1) data from 2003 to 2011 at all latitudes, which contradicts the previous finding. A follow-up

* Corresponding author.
E-mail address: anqi.li@chalmers.se (A. Li).

[1] OH_* denotes the vibrationally excited state of OH.
[2] Wind Imaging Interferometer.
[3] SCanning Imaging Absorption spectroMeter for Atmospheric CHartographY.
[4] Sounding of the Atmosphere using Broadband Emission Radiometry.

https://doi.org/10.1016/j.jastp.2022.105831
Received 9 November 2021; Received in revised form 17 January 2022; Accepted 18 January 2022
Available online 6 February 2022

study by Teiser and von Savigny (2017) used a multivariate regression method to quantify the 11-year solar cycle signature in OH (3-1) and OH(6-2). They found some evidence for an 11-year solar cycle signature in the SCIAMACHY OH(3-1) and OH(6-2) bands but only limited to the low latitude bins in specific transitional bands and are likely insignificant averaged over all latitude bins. Gao et al. (2016) studied the responses of several nightglow emissions including OH_* measured by SABER[4] to the solar radiation over a 13-year-period. This is, so far, the only spaceborne instrument that provides OH_* data covering more than 11 years. They showed that the peak emission rate and column emission rate were highly correlated with solar radiation, while the responses of the peak height to the solar radiation was not obvious.

The Optical Spectrograph and InfraRed Imager Systems (OSIRIS) has been continuously measuring the OH 3-1 transition of the Meinel band centred at 1.53 μm from 2001 to 2015 (Li et al., 2021). The time-spam covers the second half of solar cycle 23 and the first half of cycle 24 which makes this unique OH_* data set suitable to study the 11-year solar cycle influence. However, the satellite's sun-synchronous orbit has drifted in local time oscillating approximately one hour back and forth during the mission and, unfortunately, this occurred at a similar pace to the 11-year cycle. The issue of changing sampling conditions in local solar time (LST) needs to be addressed. Indeed, the OH_* layer exhibits a nocturnal variation (Marsh et al., 2006; Ward, 1999; Zhang et al., 2001; López-González et al., 2005), so the slow variation in the recorded signal may originate from the combination of changes in solar radiation and changes in local time sampling. In this study, we address this issue by using a photochemical model. We provide basic information about the observational characteristics of Odin-OSIRIS in Section 2. In Section 3.1, we present how the solar cycle signature is manifested in the data set. We then, in Section 3.2, use the model to analyse and discuss the distorted signature. Finally, conclusions are given in Section 4.

2. The IRI measurements

The InfraRed Imager (IRI) is part of the OSIRIS instrument aboard the Odin satellite (Murtagh et al., 2002; Llewellyn et al., 2004). IRI includes three separate co-aligned imagers. One of them (channel 1) has the optical filter centred around 1.53 μm. The two other ones (channels 2 and 3) are centred around 1.27 μm. Channel 1 measures the OH (3-1) Meinel band airglow emission as well as Rayleigh scattering from the molecular air density during daytime. Each exposure (ca. 1 s) obtains a vertical profile of the airglow layer from the limb with a 1 km vertical resolution. In the study by Li et al. (2021), the limb radiance profiles were inverted to volume emission rate (VER, photons cm^{-3} s^{-1}) profiles assuming optically thin atmospheric layers. VER profiles were then fitted with a Gaussian function to estimate the layer height, thickness, peak emission rate and the zenith vertically integrated volume emission rate, or zenith emission rate (ZER, photons cm^{-2} $column^{-1}$ s^{-1}). All data can be downloaded at https://doi.org/10.5281/zenodo.4746506 (Li et al., 2021b).

The Odin satellite has been orbiting the Earth approximately 15 times a day since the launch in 2001. However, after 2016 OSIRIS has operated for only a limited portion of the orbits, mainly within the sunlit part due to a power supply unit problem. Thus, we have a little more than 15 years of the Meinel band nightglow observation. Since the emission rate during daytime is too weak to be detectable, it is not used in this study. As the satellite is on a sun-synchronous, near-terminator, near-polar orbit, the nighttime observations correspond to data in the winter hemisphere, concentrated at high latitudes. Measurements made near the equator are close to the sunset and sunrise conditions at all times. The local time ascending node (LTAN) at the equator was at 18 h at the beginning of the mission and slowly drifted to 19 h around the year 2009, then back to 18 h around the year 2017.

In this study, we limit our analysis to the measurements made in the night (i.e. solar zenith angle (SZA) larger than 96°, Li et al. (2021)) and to the ascending part of the orbits, because the measurements made in the descending part of the orbits which satisfy the condition of SZA>96° are limited to only high latitudes. Fig. 1 shows the observational characteristics of the IRI data considered in this study. There are significantly more of nightglow profiles measured per year between 2007 and 2012 than during the rest of the mission (Fig. 1a) due to changes in Odin-OSIRIS operational mode. The LST has drifted by roughly 1 h and back over the course of 15 years (Fig. 1b), with the exception of the first 3–4 years at northern high latitudes, due to the change in pointing strategy. The drifting effect can also be seen in the yearly SZA (Fig. 1c) which has changed by a maximum 6.2° at the equator and 8.4° at high northern latitudes. The seasonal variation in SZA (Fig. 1d) is the largest near the poles and smallest at the equator. The latitude-time coverage of the data is also depicted in the monthly averaged SZA plot (Fig. 1d). A similar plot but for the general observational characteristics of OSIRIS, including daytime measurements, can be found in McLinden et al. (2012) Fig. 4.

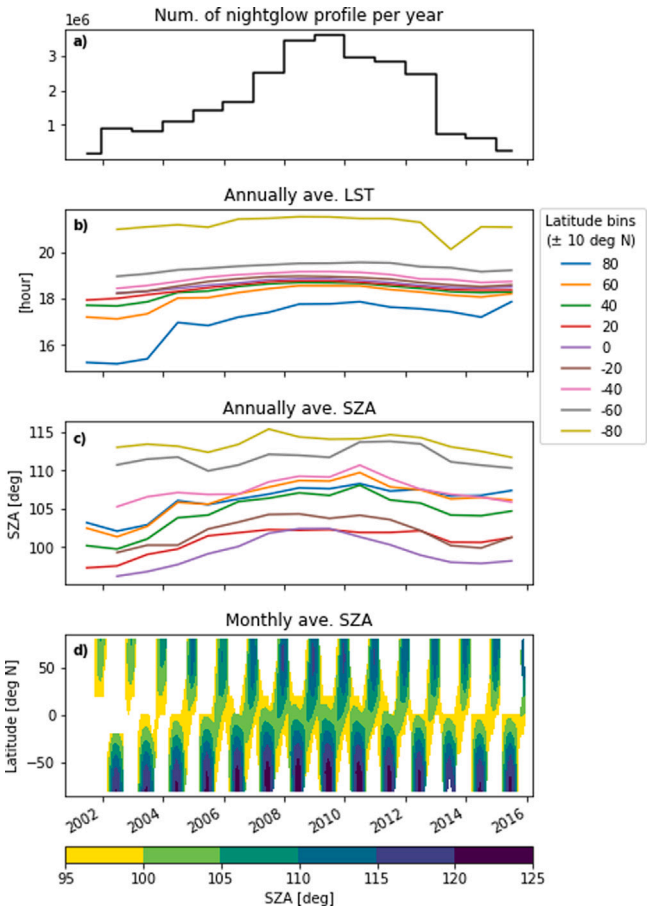

Fig. 1. Observational characteristics of IRI nighttime measurements in the ascending part of the orbit. (a) Number of nightglow profiles per year. (b) Yearly averaged local solar time (LST) at location of tangent point in 9 latitude bins. (c) Same as (b) but solar zenith angle (SZA). (d) Monthly averaged SZA in latitude-time series. White areas represent missing OSIRIS OH data.

In the next section, we analyse how the signature of the 11-year solar cycle manifested in different latitude bands, based on this global OH (3-1) nightglow data set, as well as discuss how the signature is possibly affected by the satellite drifting in LST.

3. Correlation and variability

As one of the advantages of the IRI OH (3-1) data set, the high latitude coverage with more than 15 years of observation offers us

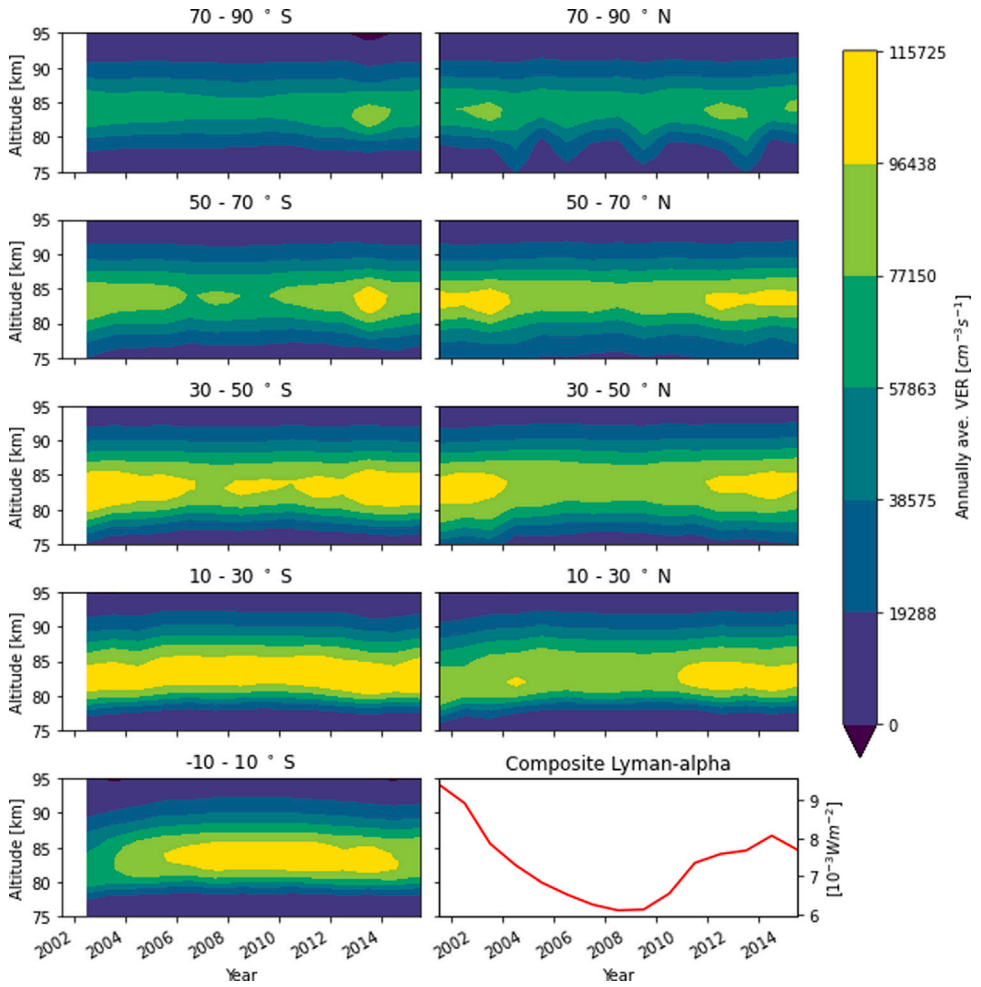

Fig. 2. Time series of the annually averaged OH (3-1) nightglow volume emission rate (VER, photons cm^{-3} s^{-1}) (see titles on top of each panels for the latitude ranges) and the annually averaged composite Lyman-α flux (red line, last panel). Note that only a limited number of months of each year are available at mid- to high latitudes (see Fig. 1d for the spatio-temporal coverage of the nightglow data).

an excellent opportunity to investigate the solar influence near the mesopause region. However, it should be noted that although the nightglow layer has a high local time dependency, the Odin measurements are relatively constant in LST in a fixed latitude due to the sun-synchronous orbit. Thus, the analysis in this paper applies to the measurements made around a certain LST (see Fig. 1). We first present the long term variability recorded by OSIRIS and its apparent signature related to the 11-year solar cycle in Section 3.1. In Section 3.2, we address the effect of the slight drifting in the observational conditions over the course of 15 years.

Firstly, we make daily averages of VER, emission height and ZER following the screening recommendations in Li et al. (2021). In this way, we prevent days with higher sampling density from dominating the annual averages. The data are binned in 20° latitude bins thus 9 bins in total. Only the data corresponding to a SZA larger than 96° and taken during the ascending part of the orbit are considered in this study. In addition, we use the composite Lyman-α time series from Machol et al. (2019)[5] to analyse the correlation with the OH nightglow characteristics. The Lyman-α flux time series is also provided in a daily average format.

Thereafter, we re-sample the daily averaged time series of nightglow and Lyman-α into inter-annual anomalies normalised as follows.

$$X_{mean}(doy) = \frac{1}{15}\sum_{y=2001}^{2015} X(y, doy), \tag{3}$$

$$X_{norm}(y, doy) = \frac{X(y, doy) - X_{mean}(doy)}{X_{mean}(doy)} \times 100\%, \tag{4}$$

$$X^{mean}_{norm}(y) = \frac{1}{nod(y)}\sum_{doy=1}^{nod(y)} X_{norm}(y, doy), \tag{5}$$

$$X^{sd}_{norm}(y) = \sqrt{\frac{1}{nod(y)}\sum_{doy=1}^{nod(y)} (X_{norm}(y, doy) - X^{mean}_{norm}(y))^2} \tag{6}$$

where y, doy and $nod(y)$ denote year, day of the year and number of measurement days in that year, respectively. X can be any of the OH_* parameters or the Lyman-α flux. $X_{mean}(doy)$ represents the daily mean value averaged over the 15 years of observation, that is mostly dominated by the seasonal variation. $X_{norm}(y, doy)$ represents the normalised anomalies. $X^{mean}_{norm}(y)$ and X^{sd}_{norm} are the mean and standard deviation of the normalised inter-annual anomalies. All quantities in the following analyses are in % unless otherwise stated.

3.1. 11-year solar cycle signature manifested in IRI OH data

Fig. 2 shows the annually averaged time series of the nightglow profiles in 9 latitude bins (with a 20° range) from 2001 to 2015. Note

[5] The composite Lyman-α data have been downloaded from https://lasp.colorado.edu/lisird/data/composite_lyman_alpha/. Last access: Jan 2021.

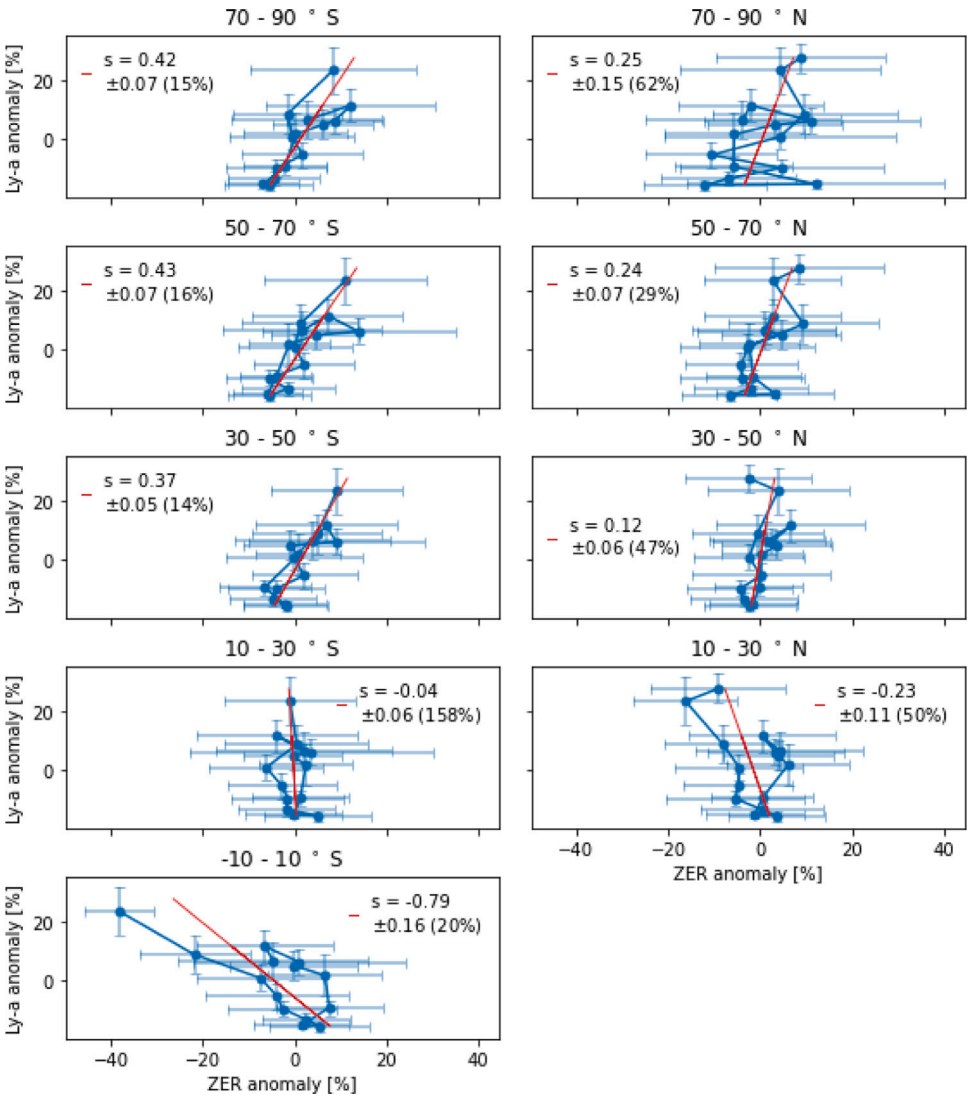

Fig. 3. Normalised inter-annual anomalies of the zenith emission rate (ZER) of the OH (3-1) nightglow layer based on IRI measurements versus the composite Lyman-α (Ly-a) flux. The latitude range is indicated in the title on top of each panel. The mean and standard deviation of normalised inter-annual anomalies are represented by the blue dots and error bars, respectively. The red line is the linear regression based on the values for each latitude bin. The slope, s, and its uncertainty based on the linear fit are indicated in the legend of each plot (in units of %/%).

that the summer seasons are not included at mid- to high latitudes (see Fig. 1d). The annually averaged composite Lyman-α flux is also plotted at the bottom right of Fig. 2 as a reference to the 11-year solar cycle. At latitudes between 30 and 70° in both hemispheres, the VER inter-annual variations clearly mirror the solar cycle — with a minimum nightglow emission rate in the years when Lyman-α flux was at minimum, and vice versa. In the polar regions (70–90 ° S and N), the same signature is present but less clear in comparison with the mid latitudes. However, at latitudes lower than 30° the same signature is unclear or even reversed in the equatorial region (10 ° S - 10 ° N) — with a maximum emission rate at solar minimum, and vice versa. It is also worth to point out that the large variations seen at the north pole is caused by the 4 major sudden stratospheric warming (SSW) events in, namely, 2004, 2006, 2009 and 2013, but this will not be the focus of this study.

For a more quantitative measure of the correlation between the nightglow layer and the solar cycle, we look at the scatter plots of the normalised inter-annual anomalies of OH (3-1) ZER versus the Lyman-α flux in each latitude range. Note that ZER here is the zenith integral of the fitted Gaussian VER profile as described in Li et al. (2021) and included in the data set (Li et al., 2021b). The correlation is shown in Fig. 3. The dots represent the mean and the error bars represent the inter-annual standard deviation such as the variability caused by the major SSW events at the north pole. We use the annual means to perform a simple linear regression to calculate the slope value, s, in the unit of %/%, which is indicated in each panel. Similar to the study done by von Savigny (2015), Fig. 8, the uncertainty of the slope is also computed based on the linear regression. In most latitude ranges in the southern hemisphere, the slope uncertainty is smaller than 20%, except at the mid to low latitude (10–30 S) since the slope itself is extremely small. The slope uncertainty is larger in the northern hemisphere due to higher variability of atmospheric dynamics. The slopes are all positive at latitudes higher than 30°, with higher values in the southern hemisphere. However, the slope flips to negative at the equator (10° S - 10° N) as the negative correlation is also visible in Fig. 2 to the unaided eye, and at the mid-low latitudes (10–30° N and S). Moreover, at latitudes lower than 30°, the scatter plots present a binary structure, where the slope corresponding to the first half of the solar cycle is different from the one corresponding to the second half of the cycle. In the next section, we analyse and discuss the possible reasons for the reversal of the positive correlation at low latitudes.

As might be expected from the previously demonstrated anti-correlation between the emission height and emission rate

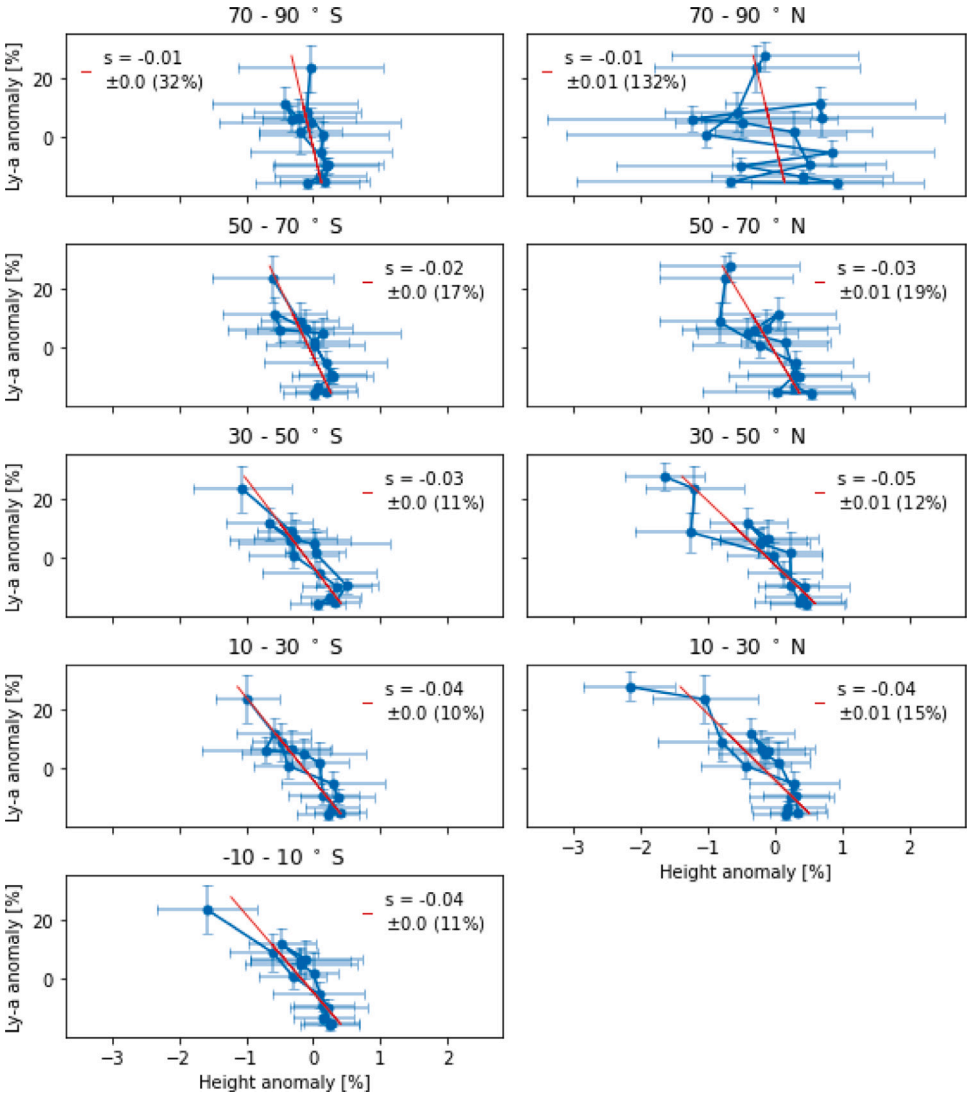

Fig. 4. Same as Fig. 3 but for OH (3-1) emission height.

(Grygalashvyly, 2015; Liu and Shepherd, 2006a; von Savigny, 2015), Fig. 4 shows that the emission height has a negative response with respect to the Lyman-α flux at all latitudes. Note that the emission height is estimated from a Gaussian fit approach and it is included in the data set (Li et al., 2021b). The uncertainty in the slopes is lower than 32% everywhere, except in the northern polar latitudes, where the variability is significantly more important due to several years affected by major SSWs. However, since the slope direction of the emission rate flips around the equator (Fig. 3), this points to an inconsistency with the anti-correlation between OH emission rate and layer height found in previous studies. Since the OSIRIS observations at low latitudes seem to be at odds with the empirical relationship, we suspect that something is affecting the data.

3.2. Analysis and discussion

The positive correlation of the airglow emission rate with the Lyman-α flux is expected. As discussed in Sonnemann et al. (2015), atomic oxygen and temperature are the basic influences on the OH_* layer emission rate. In the years of solar maximum, a stronger photodissociation of molecular oxygen into atomic oxygen results in an enhanced production of OH_*. The positively correlated solar cycle signature is clearly imprinted in their numerical experiment data (shown in their Fig. 4). Observational evidence can also be found in von Savigny (2015) Fig. 8 (left column for the zenith emission rates), although their main conclusion, based on the emission height (right column), is that there is no obvious correlation in comparison to the earlier study by Liu and Shepherd (2006a). Other observational studies which also show the airglow emission rate positively correlated with the solar cycle include (Wiens and Weill, 1973; Fukuyama, 1977; Pertsev and Perminov M. Obukhov, 2008; Clemesha et al., 2005). These studies are mainly based on ground-based observations since long term monitoring is relatively easier to achieve compared to space-born instruments.

The negative correlation of the airglow emission height with the Lyman-α flux is also expected. As discussed in Grygalashvyly et al. (2014) (see Fig. 12), an enhanced photodissociation of molecular oxygen results in a downward shift of constant isosurfaces of ozone and atomic hydrogen, thus a downward shift in OH_* production. Their model results show that the emission height variation of OH_* with the 11-year solar cycle amounts to 200–700 m depending on the season and latitude, which slightly lower than our observational data in Fig. 4 corresponding to a 500–1500 m variation.

The main question – regarding the OH(3-1) emission rate observed by OSIRIS (Fig. 3) – is: why is the positive correlation with the solar radiation reversed at low latitudes? The answer may lie in the Odin observational drift over the years, in combination with the large local time dependence of the OH_* layer, especially around the equator.

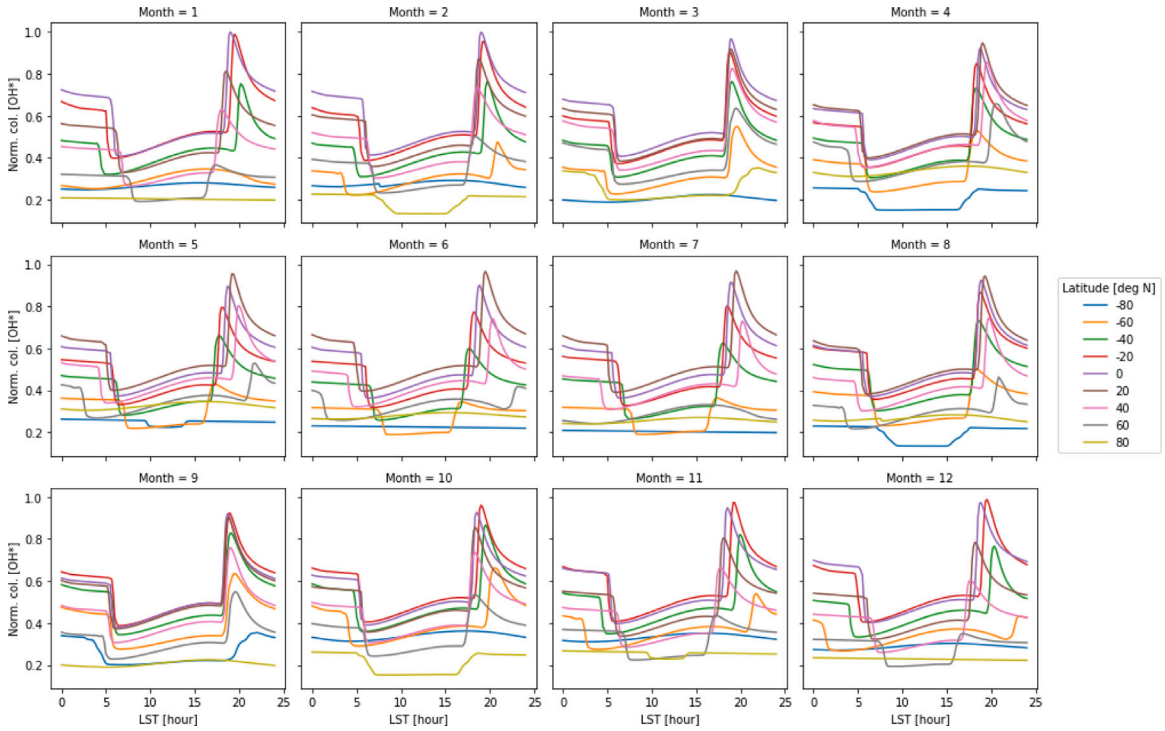

Fig. 5. Modelled diurnal variations of the column OH_*. Values are normalised by the average in each latitude and day. The title on top of each panel indicates the month of the year and the colours of the lines represent the different latitudes.

Among others, Zhang and Shepherd (1999), Liu and Shepherd (2006b), Marsh et al. (2006) demonstrated the large local time dependence of the OH_* nightglow based on the observations from SABER and WINDII. As discussed in Section 2, Odin observations are relatively fixed in local time for a given latitude, but have been drifting away by approximately one hour into the night and back. The equatorial crossing time was around 18:00 in 2001, drifted to 19:00 in 2009 and then drifted back to 18:00 in 2015. Unfortunately, this drift is synchronised with the solar cycle. It is difficult to separate the influence of the changing solar flux and of the sampling conditions without a sophisticated model.

The modelling efforts by using TIME (Zhang et al., 2001) and ROSE (Marsh et al., 2006) attribute the local time variations mainly to the tidal influence. However, according to Marsh et al. (2006) Fig. 11 and 12, one can argue that, around the sunset hours, the photochemical effect dominates the nocturnal variation before being overrun by the tidal influence. Therefore, we use a time dependent photochemical model to investigate the relative change in OH_* density due to the sampling shift of Odin. The photochemical model is derived from Allen et al. (1984), and includes the most important processes of the O_X ($O+O_3$) and HO_X ($H+OH+HO_2$) families in the mesosphere to predict the diurnal variations of H and O_3 between 75 and 95 km in 12 months and 9 latitudes (with 20° apart).

Then, we use a simplified OH_* model to approximate the $[OH_*]$ profile,

$$[OH*] = \frac{k_{H+O_3}[H][O_3]}{k_{OH+M}([N2]+[O_2]+[O])}, \quad (7)$$

where [X] denotes the concentration of species X, k_{H+O_3} is the rate constant of the reaction $H+O_3 \rightarrow OH_*+O_2$ and k_{OH+M} is the quenching rate of OH_* following the "sudden death" model in McDade and Llewellyn (1987). Finally, the zenith vertically integrated $[OH_*]$ profile is normalised to obtain a proxy for the diurnal variation of the OH_* ZER. The result is shown in Fig. 5.

The modelled column density of OH_* in different months and latitudes allows us to quantify the change in observed OH_* ZER resulting purely from the Odin observational drift in LST. We sample the modelled results based on the Odin observational pattern in LST, latitude and month to obtain a time series of daily averaged OH_*. Thereafter, we followed the same procedure described in Eq. (3)–(6) (as in Fig. 3) to plotted it against the composite Lyman-α flux (Fig. 6). The equatorial region indeed shows a strong negative slope which disappears in the polar regions. Moreover, the separation between the first and second half of the solar cycle seen in Fig. 3 at equatorial latitudes appears also here in Fig. 6, in the corresponding panel. Note that the model includes only the photochemical processes. If dynamical processes such as diurnal tides were included, the negative slopes at low latitudes would be expected to be even larger according to Marsh et al. (2006) Fig. 11.

Fig. 7 summarises all slope values indicated in Fig. 3, Fig. 4 and Fig. 6. We attempt to correct the slopes corresponding to the observed ZER by subtracting the modelled effect of the drift in Odin LST sampling. The resulting slope is around 0.3–0.4 at southern mid to high latitudes and around 0.2 at northern high latitudes. The inter-hemispherical differences agrees with the SABER results shown in Gao et al. (2016). At the equator and northern low latitude the slope remain negative but the magnitude has been reduced. This is possibly due to a limitation of the model which includes photochemical processes only. Contrary to Gao et al. (2016), we observe a consistent negative response in the emission height to the solar radiation, with a larger magnitude at mid to low latitudes than at high latitudes.

Regarding the observed OH(3-1) emission height (in Fig. 4) and the fact that the slope does not reverse near the equator as observed in the ZER (Fig. 3), photochemical processes alone do not alter the OH* peak altitude over the course of a day. Thus, the change in LST sampling does not affect the observed altitude correlation with the Lyman-α flux. Furthermore the absence of "abnormal" separation near the equator, as seen in the ZER plot in Fig. 3, between the first and second half of the solar cycle supports this assertion. However, the underlying assumption above is that the photochemical effect dominates the local time variation of OH_* at least for the relevant observation times. Yee et al. (1997) and Ward (1999) have shown that the nocturnal variation in emission height largely results from tides. The degree to which the tidal effect contributes to our observed solar cycle trend around

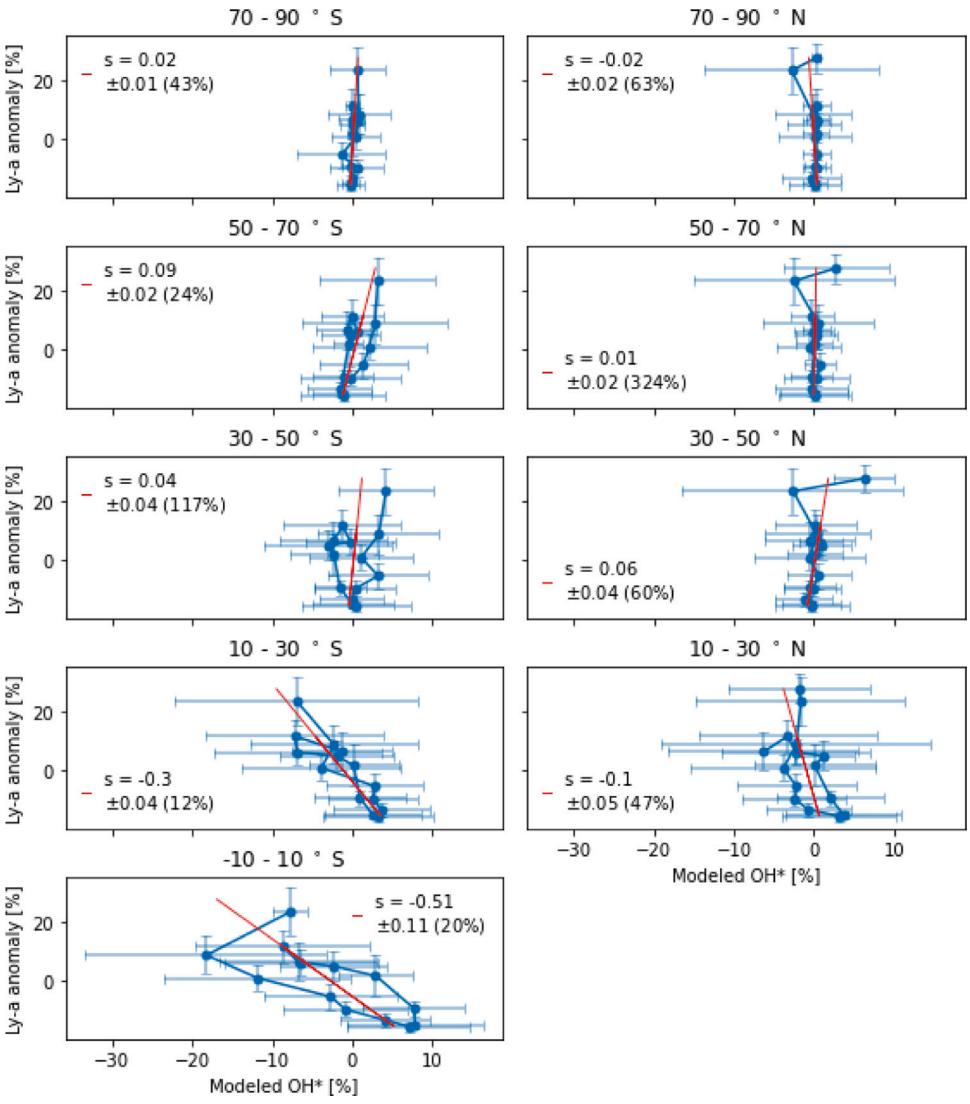

Fig. 6. Similar to Fig. 3, but with the modelled column density of OH_* following the same local solar time condition as Odin at each latitude.

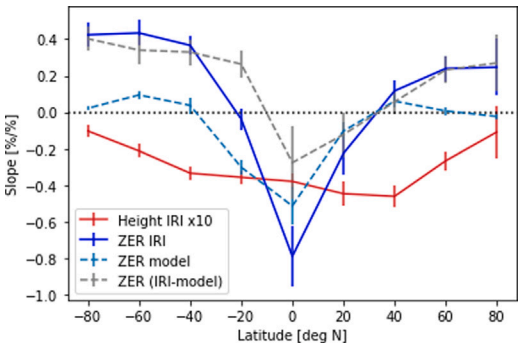

Fig. 7. Summary of all slopes presented in Fig. 3, Fig. 4 and Fig. 6, labelled as ZER IRI (blue solid), Height IRI (red solid) and ZER model (blue dash), respectively. Note that the slope for height is magnified by 10 times. The slope corresponding to the observed ZER from which was subtracted the one corresponding to the modelled ZER is labelled as ZER (IRI-model) (grey dash).

the sunset hours is still an open question, and a more sophisticated dynamical model would be needed to address the issue.

4. Conclusions

In this study, we use the OH data set which covers 15 years of OSIRIS observations (Li et al., 2021) to investigate the 11-year solar cycle influence on the OH nightglow. In general, we observe a clear 11-year solar cycle signature in the OSIRIS OH(3-1) emission and altitude. The data show a positive correlation with the Lyman-α flux in zenith emission rate at most latitudes, and a negative correlation for the emission height at all latitudes. This is consistent with previous studies of the 11-year solar cycle influence on the OH* layer. The theoretical basis is that an enhanced oxygen photolysis results in an increased atomic oxygen production, as well as a downward shift in constant isosurfaces of ozone and atomic hydrogen (Grygalashvyly et al., 2014; Sonnemann et al., 2015).

Unfortunately, the local time sampling of the Odin satellite has drifted by approximately one hour back and forth in a manner which is synchronised with the 11-year solar cycle. In addition, the OH* layer has a large nocturnal variation due to photochemistry and dynamics. Consequently, the solar cycle trend observed by OSIRIS is distorted especially near the equator where the OH* layer is expected to have the largest variation during nighttime.

To address this issue of changing sampling conditions, we have used a simple time dependent photochemistry model to simulate the OH* layer, sampling the model data under the same local solar time conditions for each latitude, during the mission operational time. Then we have associated the modelled column density of OH* with the Lyman-α flux throughout the time series and have performed a correlation analysis. The results show a prominent negative trend near the equator, which explains why the OSIRIS observed trend in terms of zenith emission rate is distorted and differs from middle and high latitudes. Extra credence to this hypothesis is given by the dichotomy in the relationship for the two phases of the solar cycle in both the observations and the model.

The same kind of distortion in the observed emission height is not expected nor observed. Because the OH* layer height has little nocturnal variation as a result of the chemistry alone. However, the above analysis is based on the assumption that dynamical effects are negligible at the local time when Odin was passing. A more detailed quantification would require a sophisticated OH* model with the inclusion of, e.g., tidal effects.

CRediT authorship contribution statement

Anqi Li: Prepared all of the calculations and figures, Discussions. **Donal P. Murtagh:** Discussions. **Adam E. Bourassa:** Produced the calibrated IRI data, Discussions. **Douglas A. Degenstein:** Produced the calibrated IRI data, Discussions. **Chris Z. Roth:** Produced the calibrated IRI data, Discussions.

Declaration of competing interest

The authors declare that they have no known competing financial interests or personal relationships that could have appeared to influence the work reported in this paper.

Acknowledgements

We would like to thank Pablo Martínez Córdova who has contributed to the implementation of the photochemical model. Odin is a Swedish-led satellite project funded jointly by the Swedish National Space Agency (SNSA), the Canadian Space Agency (CSA), the National Technology Agency of Finland (Tekes), and the Centre National d'Etudes Spatiales (CNES) in France. Odin is also part of the ESA's third party mission programme.

References

Allen, M., Lunine, J.I., Yung, Y.L., 1984. The vertical distribution of ozone in the mesosphere and lower thermosphere. J. Geophys. Res. 89 (D3), 4841–4872.

Clemesha, B., Takahashi, H., Simonich, D., Gobbi, D., Batista, P., 2005. Experimental evidence for solar cycle and long-term change in the low-latitude MLT region. J. Atmos. Solar-Terr. Phys. 67 (1–2), 191–196. http://dx.doi.org/10.1016/j.jastp.2004.07.027.

Fukuyama, K., 1977. Airglow variations and dynamics in the lower thermosphere and upper mesosphere-II. Seasonal and long-term variations. J. Atmos. Solar-Terr. Phys. 39 (1), 1–14. http://dx.doi.org/10.1016/0021-9169(77)90038-1.

Gao, H., Xu, J., Chen, G.M., 2016. The responses of the nightglow emissions observed by the TIMED/SABER satellite to solar radiation. J. Geophys. Res. A: Space Phys. 121 (2), 1627–1642. http://dx.doi.org/10.1002/2015JA021624.

García-Comas, M., José López-González, M., González-Galindo, F., Luis de la Rosa, J., López-Puertas, M., Shepherd, M.G., Shepherd, G.G., 2017. Mesospheric OH layer altitude at midlatitudes: variability over the Sierra Nevada observatory in Granada, Spain (37 ° N, 3 ° W) 35. Ann. Geophys. 1151–1164. http://dx.doi.org/10.5194/angeo-35-1151-2017.

Grygalashvyly, M., 2015. Several notes on the OH* layer. Ann. Geophys. 33 (7), 923–930. http://dx.doi.org/10.5194/angeo-33-923-2015.

Grygalashvyly, M., Sonnemann, G.R., Lübken, F.J., Hartogh, P., Berger, U., 2014. Hydroxyl layer: Mean state and trends at midlatitudes. J. Geophys. Res. 119 (21), 12,391–12,419. http://dx.doi.org/10.1002/2014JD022094.

Li, A., Roth, C.Z., Bourassa, A.E., Degenstein, D.A., Pérot, K., Christensen, O.M., Murtagh, D.P., 2021. The OH (3-1) nightglow volume emission rate retrieved from OSIRIS measurements: 2001 to 2015. Earth Syst. Sci. Data Discuss. 2021a, 1–18. http://dx.doi.org/10.5194/essd-2021-191.

Li, A., Roth, C.Z., Pérot, K., Christensen, O.M., Bourassa, A.E., Degenstein, D.A., Murtagh, D., 2021b. OH (3-1) nightglow volume emission rate and its characteristics based on OSIRIS measurements. http://dx.doi.org/10.5281/ZENODO.4746506.

Liu, G., Shepherd, G.G., 2006a. An empirical model for the altitude of the OH nightglow emission. Geophys. Res. Lett. 33 (9), http://dx.doi.org/10.1029/2005GL025297.

Liu, G., Shepherd, G.G., 2006b. Perturbed profiles of oxygen nightglow emissions as observed by WINDII on UARS. J. Atmos. Solar-Terr. Phys. 68 (9), 1018–1028. http://dx.doi.org/10.1016/j.jastp.2005.12.004.

Llewellyn, E.J., Lloyd, N.D., Degenstein, D.A., Gattinger, R.L., Petelina, S.V., Bourassa, A.E., Wiensz, J.T., Ivanov, E.V., McDade, I.C., Solheim, B.H., McConnell, J.C., Haley, C.S., von Savigny, C., Sioris, C.E., McLinden, C.A., Griffioen, E., Kaminski, J., Evans, W.F.J., Puckrin, E., Strong, K., Wehrle, V., Hum, R.H., Kendall, D.J.W., Matsushita, J., Murtagh, D.P., Brohede, S., Stegman, J., Witt, G., Barnes, G., Payne, W.F., Piché, L., Smith, K., Warshaw, G., Deslauniers, D.L., Marchand, P., Richardson, E.H., King, R.A., Wevers, I., McCreath, W., Kyrölä, E., Oikarinen, L., Leppelmeier, G.W., Auvinen, H., Mégie, G., Hauchecorne, A., Lefèvre, F., de La Nöe, J., Ricaud, P., Frisk, U., Sjoberg, F., von Schéele, F., Nordh, L., 2004. The OSIRIS instrument on the odin spacecraft. Can. J. Phys. 82 (6), 411–422. http://dx.doi.org/10.1139/p04-005.

López-González, M.J., Rodríguez, E., Shepherd, G.G., Sargoytchev, S., Shepherd, M.G., Aushev, V.M., Brown, S., García-Comas, M., Wiens, R.H., 2005. Tidal variations of O 2 atmospheric and OH(6-2) airglow and temperature at mid-latitudes from SATI observations. Ann. Geophys. 23, 3579–3590.

Machol, J., Snow, M., Woodraska, D., Woods, T., Viereck, R., Coddington, O., 2019. An improved Lyman-alpha composite. Earth Space Sci. 6 (12), 2263–2272. http://dx.doi.org/10.1029/2019EA000648.

Marsh, D.R., Smith, A.K., Mlynczak, M.G., Russell, J.M., 2006. SABER Observations of the OH meinel airglow variability near the mesopause. J. Geophys. Res.: Space Phys. 111 (10), http://dx.doi.org/10.1029/2005JA011451.

McDade, I.C., Llewellyn, E.J., 1987. Kinetic parameters related to sources and sinks of vibrationally excited OH in the nightglow. J. Geophys. Res. 92 (A7), 7643. http://dx.doi.org/10.1029/ja092ia07p07643.

McLinden, C.A., Bourassa, A.E., Brohede, S., Cooper, M., Degenstein, D.A., Evans, W.J., Gattinger, R.L., Haley, C.S., Llewellyn, E.J., Lloyd, N.D., Loewen, P., Martin, R.V., McConnell, J.C., McDade, I.C., Murtagh, D., Rieger, L., Von Savigny, C., Sheese, P.E., Sioris, C.E., Solheim, B., Strong, K., 2012. Osiris: A decade of scattered light. Bull. Am. Meteorol. Soc. 93 (12), 1845–1863. http://dx.doi.org/10.1175/BAMS-D-11-00135.1.

Murtagh, D., Frisk, U., Merino, F., Ridal, M., Jonsson, A., Stegman, J., Witt, G., Eriksson, P., Jiménez, C., Megie, G., De la Noë, J., Ricaud, P., Baron, P., Pardo, J.R., Hauchcorne, A., Llewellyn, E.J., Degenstein, D.A., Gattinger, R.L., Lloyd, N.D., Evans, W.F., McDade, I.C., Haley, C.S., Sioris, C., Von Savigny, C., Solheim, B.H., McConnell, J.C., Strong, K., Richardson, E.H., Leppelmeier, G.W., Kyrölä, E., Auvinen, H., Oikarinen, L., 2002. An overview of the Odin atmospheric mission. Can.. J. Phys. 80 (4), 309–319. http://dx.doi.org/10.1139/P01-157.

Pertsev, N., Perminov M. Obukhov, V.A., 2008. Response of the Mesopause Airglow to Solar Activity Inferred from Measurements at Zvenigorod, Russia, Vol. 26. Tech. Rep., pp. 1049–1056, URL www.ann-geophys.net/26/1049/2008/.

Sonnemann, G.R., Hartogh, P., Berger, U., Grygalashvyly, M., 2015. Hydroxyl layer: Trend of number density and intra-annual variability. Ann. Geophys. 33 (6), 749–767. http://dx.doi.org/10.5194/angeo-33-749-2015.

Teiser, G., von Savigny, C., 2017. Variability of OH(3-1) and OH(6-2) emission altitude and volume emission rate from 2003 to 2011. J. Atmos. Solar-Terr. Phys. 161, 28–42. http://dx.doi.org/10.1016/j.jastp.2017.04.010.

von Savigny, C., 2015. Variability of OH(3-1) emission altitude from 2003 to 2011: Long-term stability and universality of the emission rate-altitude relationship. J. Atmos. Solar-Terr. Phys. 127, 120–128. http://dx.doi.org/10.1016/j.jastp.2015.02.001.

Ward, W.E., 1999. A simple model of diurnal variations in the mesospheric oxygen nightglow. Geophys. Res. Lett. 26 (23), 3565–3568. http://dx.doi.org/10.1029/1999GL003661.

Wiens, R.H., Weill, G., 1973. Diurnal, annual and solar cycle variations of hydroxyl and sodium nightglow intensities in the Europe-Africa sector. Planet. Space Sci. 21 (6), 1011–1027. http://dx.doi.org/10.1016/0032-0633(73)90147-5.

Yee, J.H., Crowley, G., Roble, R.G., Skinner, W.R., Burrage, M.D., Hays, P.B., 1997. Global simulations and observations of O(1S), O2(1$\sum$) and OH mesospheric nightglow emissions. J. Geophys. Res. A: Space Phys. 102 (A9), 19949–19968. http://dx.doi.org/10.1029/96JA01833.

Zhang, S.P., Roble, R.G., Shepherd, G.G., 2001. Tidal influence on the oxygen and hydroxyl nightglows: Wind imaging interferometer observations and thermosphere/ionosphere/mesosphere electrodynamics general circulation model. J. Geophys. Res.: Space Phys. 106 (A10), 21381–21393. http://dx.doi.org/10.1029/2000ja000363.

Zhang, S.P., Shepherd, G.G., 1999. The influence of the diurnal tide on the O(1S) and OH emission rates observed by WINDII on UARS. Geophys. Res. Lett. 26 (4), 529–532. http://dx.doi.org/10.1029/1999GL900033.